BASIC SCIENCE

Nanomedicine: Nanotechnology, Biology, and Medicine
23 (2020) 102113

Original Article

nanomedjournal.com

PEGylated mucus-penetrating nanocrystals for lung delivery of a new FtsZ inhibitor against *Burkholderia cenocepacia* infection

Gabriella Costabile, PhD[a], Romina Provenzano, MSci[a], Alberto Azzalin, PhD[b], Viola Camilla Scoffone, PhD[b], Laurent R. Chiarelli, PhD[b], Valeria Rondelli, PhD[c], Isabelle Grillo, PhD[d], Thomas Zinn, PhD[e], Alexander Lepioshkin, MSci[f], Svetlana Savina, MSci[f], Agnese Miro, MSci[a], Fabiana Quaglia, PhD[a], Vadim Makarov, PhD[f], Tom Coenye, PhD[g], Paola Brocca, PhD[c], Giovanna Riccardi, MSci[b], Silvia Buroni, PhD[b,*], Francesca Ungaro, PhD[a,*]

[a]*Department of Pharmacy, University of Napoli "Federico II", Napoli, Italy*
[b]*Department of Biology and Biotechnology "L. Spallanzani", University of Pavia, Pavia, Italy*
[c]*Department of Medical Biotechnologies and Translational Medicine (BioMeTra), University of Milan, Segrate, (MI), Italy*
[d]*Institut Laue-Langevin, Grenoble, France*
[e]*ESRF-The European Synchrotron, Grenoble, France*
[f]*Federal Research Centre "Fundamentals of Biotechnology" of the Russian Academy of Sciences, Moscow, Russia*
[g]*Laboratory of Pharmaceutical Microbiology, Ghent University, Ghent, Belgium*

Revised 16 September 2019

Abstract

C109 is a potent but poorly soluble FtsZ inhibitor displaying promising activity against *Burkholderia cenocepacia*, a high-risk pathogen for cystic fibrosis (*CF*) sufferers. To harness C109 for inhalation, we developed nanocrystal-embedded dry powders for inhalation suspension consisting in C109 nanocrystals stabilized with D-α-tocopheryl polyethylene glycol 1000 succinate (TPGS) embedded in hydroxypropyl-β-cyclodextrin (CD). The powders could be safely re-dispersed in water for *in vitro* aerosolization. Owing to the presence of a PEG shell, the rod shape and the peculiar aspect ratio, C109 nanocrystals were able to diffuse through artificial *CF* mucus. The promising technological features were completed by encouraging *in vitro*/*in vivo* effects. The formulations displayed no toxicity towards human bronchial epithelial cells and were active against planktonic and sessile *B. cenocepacia* strains. The efficacy of C109 nanosuspensions in combination with piperacillin was confirmed in a *Galleria mellonella* infection model, strengthening their potential for combined therapy of *B. cenocepacia* lung infections.

Key words: Nanocrystals; Polyethylene glycol; TPGS; Cyclodextrin; Lung delivery; Burkholderia cenocepacia; Mucus; Cystic fibrosis

Cystic Fibrosis (*CF*) is a fatal inherited disease which causes the formation of thick and sticky mucus in the lungs, leading to serious infections in *CF* sufferers, with chronic inflammation, progressive lung damage, and premature death.[1] To extend the life expectancy of *CF* patients, it is mandatory to control infections and inflammation.[2,3] Nonetheless, *CF* pathogens are naturally multidrug resistant to antibiotics and can form biofilms in the airways, thus increasing their tolerance to drugs.[2,3]

Among the opportunistic pathogens able to colonize *CF* lung, *Burkholderia cenocepacia* is a Gram-negative bacterium that causes an increased decline of lung function and potential fatal pneumonia.[4] *B. cenocepacia* shows resistance to numerous classes of antibiotics.[5] Moreover, patients colonized by *B. cenocepacia* show 50% lower post-transplant survival than non-colonized people,[6] so often they are not admitted to transplant.[7] In general, the use of combined therapy is recommended,[8] but standardized eradication protocols do not exist.[9]

Despite the high levels of resistance, there has been little progress in developing new therapeutic strategies to fight *B. cenocepacia* infections. In previous studies, a new benzothiadiazole derivative, named C109, was found to have a promising

*Corresponding authors.
E-mail addresses: silvia.buroni@unipv.it, (S. Buroni), ungaro@unina.it. (F. Ungaro).

https://doi.org/10.1016/j.nano.2019.102113

Please cite this article as: Costabile G, et al, PEGylated mucus-penetrating nanocrystals for lung delivery of a new FtsZ inhibitor against *Burkholderia cenocepacia* infection. *Nanomedicine: NBM* 2020;23:102113, https://doi.org/10.1016/j.nano.2019.102113

in vitro antibacterial activity against *B. cenocepacia*.[10] More recently, C109 was demonstrated to act as an inhibitor of the filamenting temperature-sensitive mutant Z (FtsZ) protein,[11] involved in the bacterial cell-division process.[12]

The proven anti-burkholderia activity of C109 makes this compound an interesting candidate for local treatment of lung infections in *CF* patients, who strongly benefit of aerosolized antibacterial therapies.[13] Nevertheless, inhaled C109 poses important formulation and delivery challenges because of its poor aqueous solubility. Among the available formulation options, the so-called "nanosuspensions" are colloidal dispersions of pure submicron drug particles stabilized by surfactants (*i.e.*, nanocrystals) that can help to increase drug solubility and dissolution rate in biological fluids.[14,15] For pulmonary application, an aqueous nanosuspension can be delivered through commercially available nebulizers.[16] Nonetheless, the ability of the drug nanocrystals to adequately deposit along the airways and to overcome extracellular lung barriers should be taken properly into account.[17,18] In this respect, numerous lines of evidence suggest that PEGylation may improve penetration of the nanoparticulate system inside both mucus and bacteria biofilm lining airway epithelia.[19–21] In addition, size and shape are relevant parameters governing deposition and fate within biological environments.[22,23]

The aim of this work was the development of inhalable nanosuspensions consisting in C109 nanocrystals stabilized with D-α-tocopheryl polyethylene glycol 1000 succinate (TPGS). Optimized formulations (*i.e.*, TPGS_C109) were freeze-dried with hydroxypropyl-β-cyclodextrin (CD), which has been previously demonstrated a valid cryoprotectant for PEGylated nanoparticles.[24] The developed formulations were fully characterized, paying attention to C109 nanocrystal structure, aerosol performance, interactions with mucus and *in vitro/in vivo* efficacy.

Methods

All the details of the listed methods are reported in the *Supplementary Data*.

Materials

All chemicals and reagents are described in *Supplementary Data*. Methyl [(4-nitro-2,1,3-benzothiadiazol-5-yl)thio]acetate (10,126,109; C109) was synthesized and characterized at as previously reported.[10]

Production and characterization of C109 nanosuspensions

C109 nanosuspensions were produced by nanoprecipitation. C109 (5-10 mg) was solubilized in 1 ml of organic solvent, loaded into a syringe and injected dropwise in 10 mL of aqueous TPGS (10-20 mg). The resulting dispersion was transferred in ice and sonicated by a microtip probe for 6 min at 1 W (Sonicator 3000, Misonix, USA). Afterwards, the organic solvent was removed under stirring overnight and the dispersion diluted to 10 mL with ultrapure water. When appropriate, the nanosuspension was centrifuged at 1000 rpm for 5 min (Hettich Zentrifugen, Universal 16R).

The hydrodynamic diameter (D_H), the polydispersity index (PDI) and the zeta potential (ζ) of the nanosuspensions were determined with a Zetasizer Nano ZS (Malvern Instruments, UK). C109 concentration was determined by UV–vis spectrophotometry after solubilizing an appropriate volume of nanosuspension in tetrahydrofuran.

Production and characterization of C109 nanocrystal-embedded dry powders

After addition of CD at 0.5 or 1% (w/v), optimized C109 nanosuspensions (TPGS_C109) were freeze-dried at 0.1 mbar and −80 °C (LyoQuest, Telstar Italy).

D_H, PDI and the ζ of the reconstituted nanosuspensions were determined. Nanocrystal shape and morphology were analyzed by transmission electron microscopy (TEM) upon air drying 10 μL of reconstituted nanosuspension (3 mg/ml) mounted on 200 mesh copper grids coated with carbon film. The analysis was performed with a FEI Tecnai G2 200 kV s-Twin microscope equipped with a 4 K camera (ThermoFisher Scientific, US). Fixed aqueous layer thickness (FALT) of the nanocrystals was evaluated before and after freeze-drying by monitoring the influence of NaCl (final concentration 1-15 mM) on the ζ of nanocrystals.[25]

Scattering methods

Small-angle and wide-angle x-ray scattering

TPGS_C109 nanosuspension and the corresponding freeze-dried powders were investigated at room temperature by combining small-angle (SAXS) and wide-angle X-ray scattering (WAXS) experiments. The measurements were carried out at the ESRF high brilliance SAXS beamline ID02 (Grenoble, France).[26]

Small-angle neutron scattering

Small-angle neutron scattering (SANS) experiments were performed at the Institut Laue-Langevin, ILL (Grenoble, France) using the D33 diffractometer.

In vitro aerosol performance

In vitro aerosolization properties of C109 nanocrystal-embedded dry powders for inhalation suspension were tested after delivery from different commercial nebulizers: PARI TurboBOY® (PARI GmbH, Germany), eFlow® rapid (PARI GmbH, Germany) and Aeroneb® Go (Aerogen, Ireland). The deposition pattern was investigated using a Next Generation Impactor (NGI) (Copley Scientific, UK), with sampling at 15 L/min and insertion of a filter in micro-orifice collector (MOC) as previously reported.[27]

Studies in simulated lung fluids

Simulated lung fluids composition and preparation

Simulated interstitial lung fluid (SILF) was prepared according to Marques et al.[28] The artificial *CF* mucus was achieved as previously reported.[27] A mucin type II dispersion (2% w/v) in salt-containing D_2O (4.4 mg/mL sodium chloride, 15 mg/mL potassium chloride and 3.0 mg/mL calcium chloride dehydrate) was also prepared for SANS measurements.

Evaluation of particle behavior and migration in artificial mucus

For SAXS measurements, a nanocrystal dispersion in water (10 mg/mL) was mixed with artificial *CF* mucus (1:3 v/v). Measurements were performed after 1 h equilibration time. SAXS studies of particle horizontal migration in artificial *CF* mucus were performed in the same plastic capillaries used for structural investigation by inserting 80 μL of mucus from one edge of the capillary and 20 μL of the particle dispersion from the other edge, to put them in contact inside the capillary (total interface 3.14 mm^2). Capillaries were kept horizontally, and spectra were taken during 10 h in different horizontal positions along the capillary.

For SANS measurements, the nanocrystal dispersion at 10 mg/mL was mixed with the mucin type II dispersion in salt containing D_2O (1:3 v/v). The spectra lag time after preparation was around 5 h.

C109 release in simulated lung fluids

In vitro release studies of C109 from artificial *CF* mucus to SILF were performed by membrane dialysis as previously reported.[27] Briefly, C109, TPGS_C109 (0.1 mL) or a corresponding amount of TPGS_C109_CD0.5/TPGS_C109_CD1.0 was added to 0.3 mL of artificial mucus or PBS and transferred in a dialysis bag (MWCO: 5000 Da, Spectra/Por®). Each sample was placed into 5 mL of external medium and kept at 37 °C. At scheduled time intervals, 1 mL of the external medium was withdrawn, replaced by the same amount of fresh medium and analyzed for C109 content. Triplicate experiments were performed.

In vitro antimicrobial activity

The MICs of the C109 formulations for *B. cenocepacia* J2315 (LMG 16656), K56-2 (LMG 18863), *B. cenocepacia* clinical isolates, *Escherichia coli* (ATCC 25922), *Acinetobacter baumannii* (ATCC 19606), *Klebsiella pneumoniae* (ATCC 13883), and *Staphylococcus aureus* (ATCC 25923) were determined by the microdilution method followed by resazurin colorimetric assay.[29]

Inhibitory and eradication activity of *B. cenocepacia* J2315 biofilm was evaluated as described in *Supplementary Data*.

Cytotoxicity on human bronchial epithelial cells

The viability of human bronchial epithelial cells wild type (16HBE), or homozygous for ΔF508 mutation (CFBE41o-) upon exposure to the formulations was assayed using the MTT method.[30]

In vivo antimicrobial activity

LD50 *B. cenocepacia* K56-2 (10^3 CFU/larva)[31] was injected into *G. mellonella* (Decathlon, www.decathlon.it). Larvae were divided in different groups receiving a 10-μL injection of: C109 dissolved in DMSO (20 mg/kg); TPGS_C109 (20 mg/kg); TPGS (at equivalent concentrations); piperacillin (100 mg/kg), TPGS_C109 *plus* piperacillin or the vehicles (saline or DMSO). After treatment, larvae were placed in Petri dishes in the dark at 30 °C, and scored as dead or alive after 24 h, 48 and 72 h.

Table 1
Overall properties of C109 nanocrystals.

	TPGS_C109	TPGS_C109_CD0.5	TPGS_C109_CD1.0
D_H[1] (nm ± SD^2)	823 ± 123	931 ± 111	842 ± 162
PDI[1] (A.U. ± SD^2)	0.331 ± 0.098	0.353 ± 0.075	0.382 ± 0.075
Zeta potential[1] (mV ± SD^2)	−21.2 ± 6.07	−21.8 ± 6.02	−20.1 ± 3.19
RDI[3] (A.U. ± SD^2)	-	1.166 ± 0.091	0.980 ± 0.073
C109 (mg/mL ± SD^2)	0.568 ± 0.132	-	-
C109 (% ± SD^2)	-	7.16 ± 1.17	2.79 ± 0.361

[1] Values determined by dynamic light scattering (DLS) and electrophoretic light scattering (ELS) with the Zetasizer Nano ZS (Malvern Instruments Ltd., UK).
[2] Results are expressed as mean value ± standard deviation (SD) of values collected from 3 batches (n = 3).
[3] Redispersibility index (RDI) is defined as D_Hi/D_{Hf} where D_{Hi} is the mean size of the nanosuspension prior to drying, and D_{Hf} is the corresponding value post-rehydration of the dried sample in water.

Results

Development of C109 nanocrystal-embedded dry powders

In depth formulation studies were devoted to the development of C109 nanocrystal-based dry powders to be reconstituted in aqueous medium for inhalation suspension. First, aqueous dispersions of drug nanocrystals were produced by a nanoprecipitation technique. Three variables were considered: drug solvent, C109 concentration and type of stabilizer. Optimal formulation parameters were chosen based on size, PDI and ζ of the nanocrystals. Of note, unreliable data were acquired by dynamic light scattering when using DMSO or THF as solvents, independently on C109 concentration (Table S1). The particle size distribution, as determined by laser diffraction analysis, confirmed the micrometric dimensions of the crystals, displaying D90 ~4.5 μm. The use of ethanol at 60 °C reduced particle size, though crystals with D_H higher than 1 μm were still achieved (Table S1). Nanocrystal size further increased when using hot ethanol as solvent in the presence of Pluronic® F68 as co-stabilizer either in the water or in the organic phase (D90 < 10.9 μm and D90 < 6.9 μm, respectively). The nanosuspension achieved by nanoprecipitation of a C109 hot ethanol solution in aqueous TPGS (C109/TPGS 1:2 w/w) was selected as the best candidate for further experiments. A centrifugation step allowed to select nanocrystals with a D_H of 823 ± 123 nm, acceptable PDI (~0.3) and negative ζ (Table S1).

To improve the stability of optimized TPGS_C109 nanosuspension, nanocrystal-embedded dry powders were produced by freeze-drying. When the nanocrystals underwent the lyophilization process, massive particle aggregation was observed; thus, CD was selected as cryoprotectant to be added before freeze-drying. The composition and the overall properties of the C109 formulations are listed in Table 1.

CD was added just after production to the aqueous phase of the nanosuspension at 0.5 or 1.0% w/v. In both cases, no significant differences in PDI and zeta potential of the nanosuspension before and after freeze-drying were observed (Table 1). A slight increase in the value of D_H was observed upon rehydration of TPGS_C109_CD0.5 as compared to both

TPGS_C109 and TPGS_C109_CD1.0 (Table 1). Nevertheless, the RDI value is always around 1. Of note, HPLC-MS analysis confirmed that C109 was stable over the production process (Figure S1).

Structural characterization of C109 nanocrystals

SAXS and WAXS measurements were performed to elucidate the structure of C109 nanocrystals. The measured SAXS profiles of the 1% w/v dispersion are reported in Figure 1, *A* along with those of free TPGS and CD for comparison. The high q portion of the scattering profiles was mainly contributed by free TPGS micelles and CD (when present). Of course, the TPGS_C109 spectrum (orange squares in Figure 1, *A*) clearly shows the lack of the CD contribution at high q. To devise this interpretation, the complementary SANS investigation is relevant (Figure 1, *C*). The investigated SANS spectral range is dominated by the scattering from the residual free TPGS micelles, with an increased scattering intensity at $q > 1$ nm^{-1} for the TPGS_C109_CD1.0 due to the presence of CD. SANS results, in agreement with previous studies elucidating TPGS core-shell structure,[32] suggest that CD did not affect micelle structure (Figure S2). Indeed, when reconstructing the high-q SAXS profile by summing the different contributions in proper proportion, it is possible to estimate that the amount of residual free TPGS in TPGS_C109_CD1.0 is about 13% w/w (about one-half of the total amount added in solution) and the amount of free CD is 72% w/w. Balancing the known added weights in the formulation, the nanocrystal is estimated to contribute 16% w/w to the total powder (Figure S3). To determine the structure of the nanocrystal, we consider the scattering intensity in the intermediate and low-q regions of the spectra.

A first analysis of SAXS measurements using a generalized Guinier-Porod model[33] gives evidence of the presence of large-sized and elongated-shaped structures (Table S2). The dimensionality ($3 - s$) of the structure was obtained ~2, denoting rod-like particles. The gyration radius R_g was around 100 nm. The Porod exponent ~4 is distinctive of the scattering from dispersed particles, allowing to interpret the total scattering spectrum as the sum of the scattering from the large particles (the nanocrystal), free TPGS and CD. Both SAXS (Figure 1, *A*) and SANS (Figure 1, *C* and S2, *B*) measurements give a Porod exponent of ~3.8 (*i.e.* $3 \leq P \leq 4$), that is distinctive of surface fractal structures with low roughness. For all the formulations, the particle size is not strongly affected by the presence of CD (also shown by the overlapping of the spectra of the three formulations at low q). Although very low scattering vectors are obtained at 10 m sample-detector distance, still some limitation to the analysis arises due to the size polydispersity (PDI ~0.3) of the nanocrystal, including quite long aggregates even below the acquired q range (see *Supplementary Data*).

Contemporary acquired WAXS spectra confirmed the presence of C109 crystal peaks in the formulations. Figure 1, *B* reports the representative WAXS spectra of C109 and TPGS_C109_CD1.0, which were obtained from the spectrum of the entire nanosuspension by subtraction of water, CD and TPGS contributions. Sharp peaks corresponding to those of the C109 crystal intramolecular ordering are apparent.

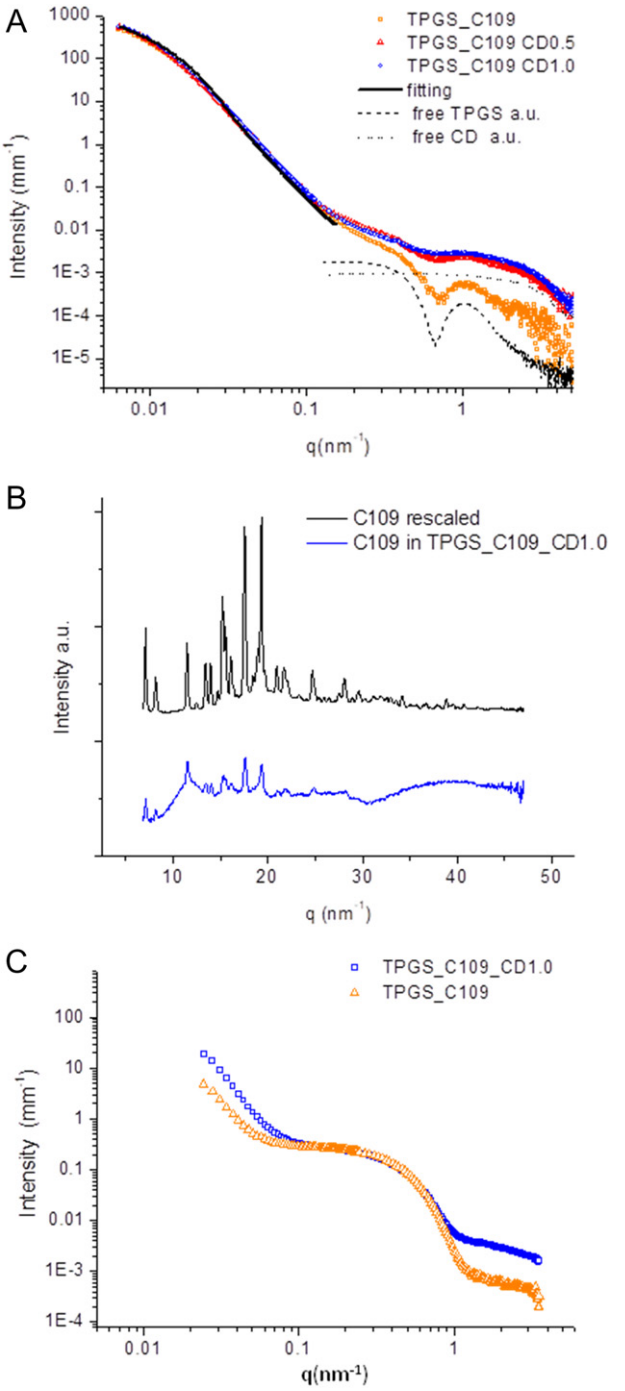

Figure 1. (**A**) SAXS spectra of TPGS_C109 (orange squares), TPGS_C109_CD0.5 (red triangles) and TPGS_C109_CD1.0 (blue circles). The black line is the fit of the lowest q region by a generalized Guinier-Porod model. The free TPGS (dotted line) and the free CD (dashed line) spectra are reported with arbitrarily rescaled intensity for the sake of comparison. (**B**) WAXS spectra of raw C109 crystals (top) and the C109 contribution to the WAXS spectrum of the TPGS_C109_CD1.0 nanosuspension (bottom). The nanocrystal contribution to the WAXS intensity was obtained after subtraction of water, TPGS and CD contributions in the right proportions. Large undulation is due to imperfect subtraction (note that C109 contribution is of the order of 1% in intensity after water subtraction). Vertical scales are arbitrary, and intensities are rescaled. (**C**) SANS spectra of TPGS_C109 (orange triangles), and TPGS_C109_CD1.0 (blue squares).

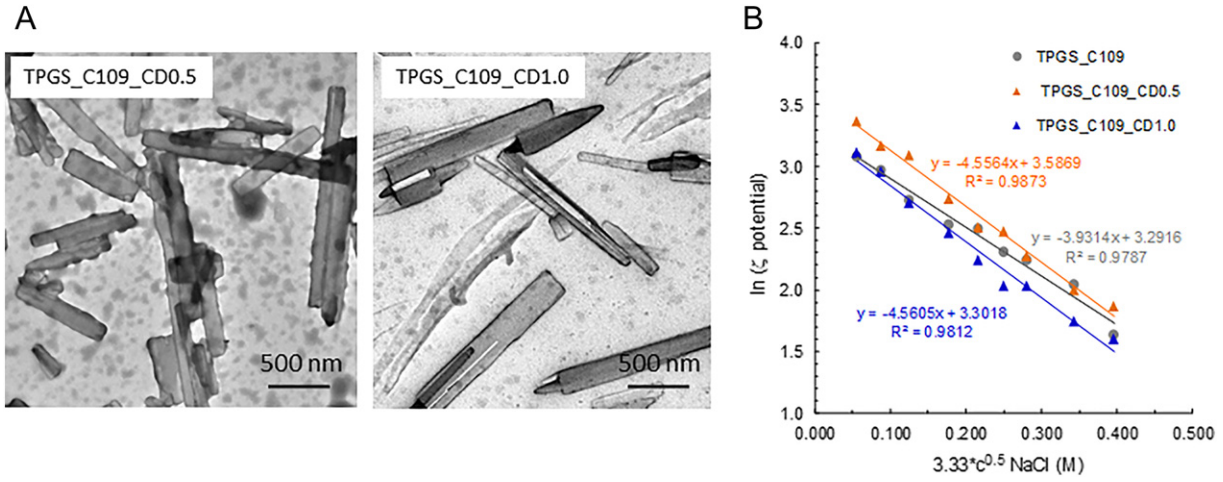

Figure 2. (**A**) TEM images of TPGS_C109_CD0.5 and TPGS_C109_CD1.0 nanocrystals after redispersion in water (field is representative of the sample). (**B**) FALT measurements of the PEG shell thickness of C109 nanocrystal formulations. The slopes of the linear regressions indicate the corresponding shell thickness in nm.

TEM analysis of TPGS_C109_CD0.5 and TPGS_C109_CD1.0 after redispersion in water confirmed a polydisperse population of elongated rod-shaped particles (Figure 2, *A*). The presence of a PEG shell on the surface of nanocrystals was confirmed by FALT measurements performed by monitoring the influence of ionic strength of the dispersing medium on particle surface charge as previously reported.[25,34] According to the Gouy-Chapmann theory, zeta-potential (ζ) decreased with increasing of the ionic strength of the medium. A plot of ln (ζ) against k ($k = 3.3\ c^{0.5}$, where k^{-1} is the Debye length) gives the thickness of the PEG polymer layer in nm as the slope of a linear regression (Figure 2). Interpolation indicates that a shell of 3.9 nm is formed on the surface of C109 nanocrystals, this value slightly increasing in the presence of CD (FALT around 4.56 nm).

In vitro aerosolization properties of C109 nanocrystal-embedded dry powders

Results achieved upon *in vitro* aerosolization of TPGS_C109_CD0.5 and TPGS_C109_CD1.0 through NGI after reconstitution of the nanosuspensions in water are reported in Figure 3.

Both TPGS_C109_CD0.5 and TPGS_C109_CD1.0 were first delivered using an advanced and handy nebulizer relying on the vibrating mesh technology (VMT) already employed in clinical practice: Aeroneb® Go (Aerogen, Ireland). Figure 3, *A* describes the cumulative droplet size distribution of the emitted dose. In both cases, the best fit line was from logarithmic linear regression ($r^2 \geq 0.98$). High fine particle fractions (FPF ~40%) and low values of experimental mass mean aerodynamic diameter ($MMAD_{exp}$ ~3 μm) were calculated, independently on CD amount in the formulation. Also, the deposition pattern of C109 throughout the NGI cups was very similar for TPGS_C109_CD0.5 and TPGS_C109_CD1.0 (Figure 3, *B*). A homogeneous distribution of the formulation throughout the seven NGI stages down to MOC was observed, with a maximum amount of the drug recovered from cups 3 and 4 (MMAD 5.39-3.3 μm).

Aerodynamic assessment of fine particles of TPGS_C109_CD1.0 was performed also after delivery from different commercial nebulizers available to *CF* patients, both conventional jet (*i.e.*, PARI TurboBOY®) and VMT (*i.e.*, eFlow® Rapid) nebulizers. Notably, the reconstituted C109 nanosuspension displayed good aerosol performance independently of the adopted nebulizer (Figure 3, *B*). Corresponding fine particle characteristics of the aerosol clouds are reported in Table 2. $MMAD_{exp}$ values ranging from 2.7 to 3.0 μm were calculated. In each case, the FPF calculated on the actual amount of C109 deposited on NGI cups with a cutoff diameter of less than 5.39 μm (cups 3-7) was ≥40%, with a maximum value ~48% in the case of the eFlow Rapid pulmonary delivery device. With respect to the emitted dose (RF in Table 2), this value increased up to 75%.

Behavior of C109 nanocrystals in simulated lung fluids

In vitro release studies were performed by dialysis from artificial *CF* mucus to SILF. A significantly increase of the release rate was observed for TPGS_C109 aqueous formulation and its dry TPGS_C109_CD0.5 and TPGS_C109_CD1.0 counterparts as compared to raw C109 (Figure 4, *A*), with 90%-95% of the initial amount of C109 added to artificial mucus available in SILF after only 2 h of incubation at 37 °C.

SAXS investigation of the behavior of the TPGS_109 formulations incubated in artificial *CF* mucus has been also performed by mixing the 10 mg/mL nanosuspensions and the model mucus in 1:3 v/v ratio. SAXS spectra were then acquired after 1 h incubation at room temperature. The reconstruction of the spectrum of the mixed system (Figure 4, *B*, black line) by linear combination of the artificial *CF* mucus (green squares) and the nanosuspension (blue squares) shows nice overlapping with the experimental profile (pink circles), except for a moderate decrease of the slope at very low-q. Similar experiments were performed by SAXS analysis of TPGS_C109 and TPGS_C109_CD0.5 formulations (Figure S3). Complementary studies were performed by SANS, allowing to exploit different contrast with respect to X-ray scattering. Figure 4, *C* shows the comparison of the SANS spectra of the initial nanocrystal formulations with the profile obtained after interaction with a 2% w/v dispersion of mucin by subtracting

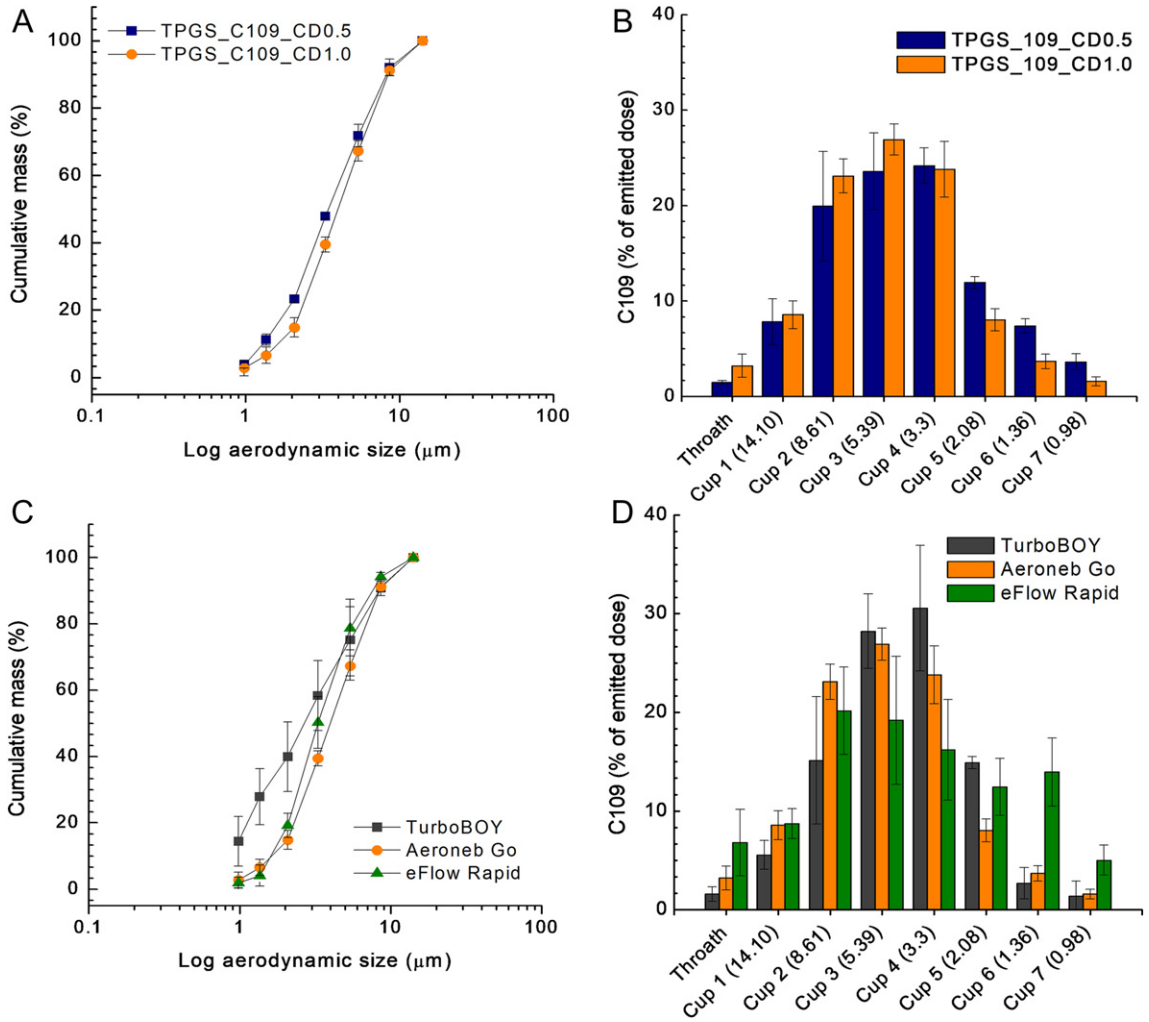

Figure 3. *In vitro* aerosol performance of TPGS_C109_CD0.5 and TPGS_C109_CD1.0 dry powders for inhalation suspension. Cumulative mass recovered as a function of the cutoff diameter (**A**) and NGI deposition pattern (**B**) upon delivery through the Aeroneb® Go nebulizer. Cumulative mass recovered as a function of the cutoff diameter (**C**) and NGI deposition pattern of TPGS_C109_CD1.0 formulation upon delivery through different nebulizers (**D**). The formulation was delivered through PARI TurboBOY® (PARI GmbH, Germany), Aeroneb® Go (Aerogen, Ireland) and eFlow® Rapid (PARI GmbH, Germany) after reconstitution in an appropriate amount of water. Data are presented as mean ± standard deviation (SD) (n = 3).

Table 2
Fine particle characteristics of the aerosol clouds generated upon delivery of the TPGS_C109_CD1.0 dry powders for inhalation suspension through different nebulizers.

	Aeroneb® Go	PARI TurboBOY®	eFlow® rapid
$MMAD_{exp}$[1] (μm ± SD)	3.04 ± 0.280	2.72 ± 0.650	2.94 ± 0.220
GSD[1] (± SD)	2.30 ± 0.060	2.83 ± 0.30	2.30 ± 0.016
FPF[2] (% ± SD)	41.9 ± 3.60	39.3 ± 4.60	47.7 ± 8.50
RF[2] (% ± SD)	63.7 ± 2.60	68.8 ± 11.6	75.0 ± 5.10

[1] Experimental MMAD and geometrical standard deviation (GSD) were calculated from the logarithmic linear regression according to European Pharmacopoeia.

[2] Percentage of particles with a MMAD lower than 5 μm. Fine Particle Fraction (FPF) was calculated on the nominal C109 dose, whereas the Respirable Fraction (RF) refers to the emitted dose of C109.

the spectral contribution of the sole mucin from that of the mixed systems. Of note, destructive effects of interaction with mucus are visible at larger scale, that is on the size of the nanocrystal. Indeed, the decrease at low q of the reconstructed difference profiles may indicate the reduction of large-scale aggregates at the time of measurement. The intensity decrease can also be associated to other effects such as a decreased correlation of the mucin mesh. However, this is unlikely to occur down to distances of 80 nm ($q \sim 0.08\ nm^{-1}$) (Figure 5, *B*). Thus, in line with release studies, SANS data suggest that the nanocrystals undergo partial dissolution upon incubation in mucin: the stronger effect of deconstruction seen in SANS with respect to SAXS can be due to the longer incubation time before analysis.

To definitively prove the ability of C109 nanocrystals to diffuse in mucus, a SAXS study of particle horizontal migration (horizontal 1D self-diffusion) was performed. Macroscopic mobility of the nanocrystal was studied in the same plastic capillaries used for structural investigation by inserting artificial *CF* mucus from one edge of the capillary and the particle dispersion from the other side (Figure 5, *A*). After 6 h of contact, SAXS spectra were collected by horizontal scanning of the capillary along its length (Figure 5, *B*). At this delay time, it was

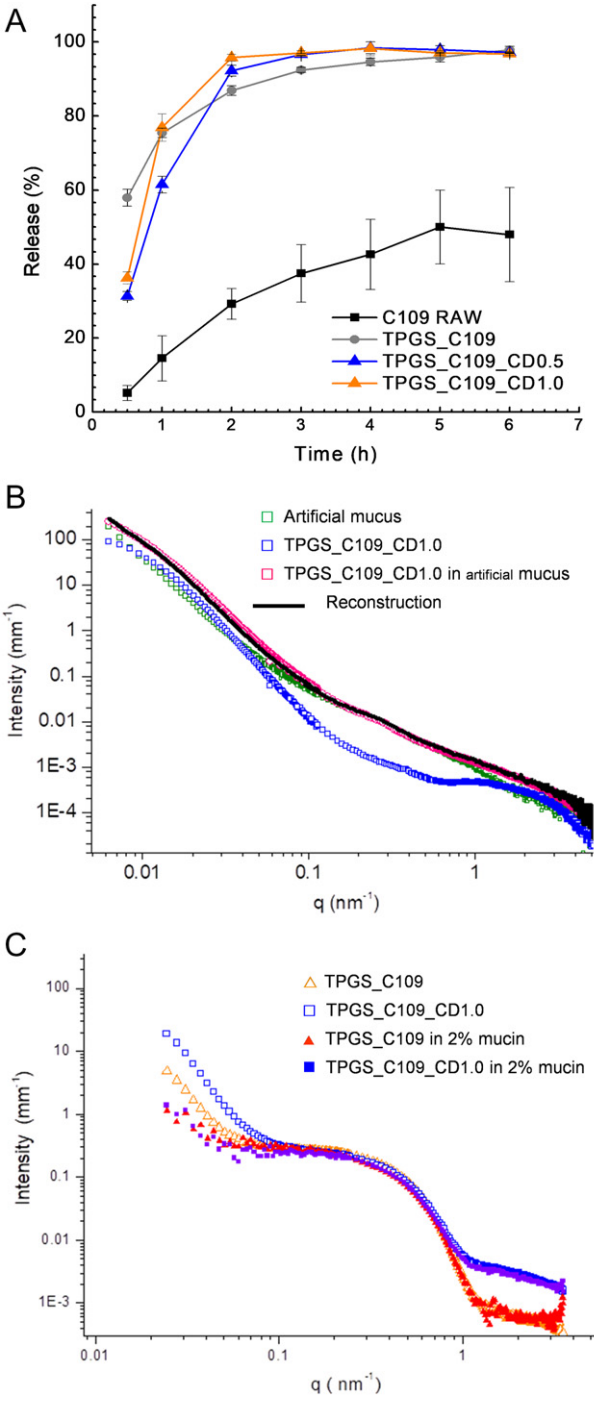

Figure 4. Behavior of nanocrystals in lung lining fluids. (**A**) *In vitro* release profile of C109 from artificial *CF* mucus to SILF at 37 °C. Data are presented as mean value ± SD (n = 3). (**B**) SAXS spectra of artificial *CF* mucus spectrum (green empty squares), TPGS_C109 (blue empty squares) and TPGS_C109_CD1.0 in artificial *CF* mucus (pink empty squares). The black lines show the spectrum reconstructed by summing the contributions of artificial *CF* mucus and TPGS_C109 CD1.0. (**C**) SANS spectra of TPGS_C109 (triangles) and TPGS_C109_CD1.0 (squares) in the 2% w/v mucin dispersion. Empty symbols are spectra of nanocrystals in water dispersion and full symbols are the spectra of the same formulations in mucin after subtraction of mucin spectral contribution to the scattered intensity.

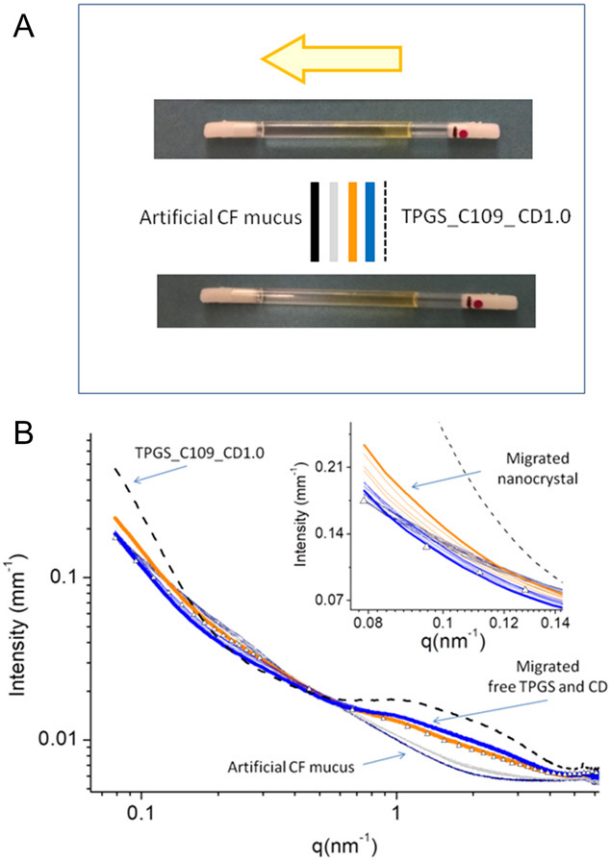

Figure 5. SAXS-assisted horizontal migration studies performed on TPGS_C109_CD1.0. (**A**) Capillary with mucus on the left and nanosuspension on the right during migration. Arrow indicates the direction of migration; bars are the color codes for spectra sequence shown in panel **B**. (**B**) Representative spectra upon a horizontal scan of the capillary from left to right. The red spectrum corresponds to a position with prevalence of low-q nanocrystal contribution with respect to the next right-side blue spectrum; triangles correspond to a spectrum taken at a longer delay after contact showing similar high-q contribution as the orange spectrum but a lower intensity at low-q (see discussion in the main text). The inset shows the low-q region scattered intensity in linear scale.

possible to macroscopically separate the different components moving with different velocities. The detection of the different components is performed by an analysis of the SAXS spectra collected at different distances from the mucus-particles initial contacting interface. The horizontal migration of the nanocrystal has a typical rate of 10 μm/min. More precise quantification is difficult due to the evolution of the nanosuspension scattering profiles during migration.

From a careful analysis of the spectra, the nanocrystal profile rises along the capillary far from the first contact interface. This is evident from the orange bold SAXS spectrum of 5, *B*, taken at about 5 mm distance from the initial mucus–particles interface: in the low-q region of the spectrum the excess scattered intensity with respect to that of sole artificial mucus is a sign of the nanocrystal presence. Reversely, the high q region of the spectrum corresponds to the amount of TPGS and CD. The amount of these last components is higher at lower migration distances from the initial interface of contact (bold blue line) and

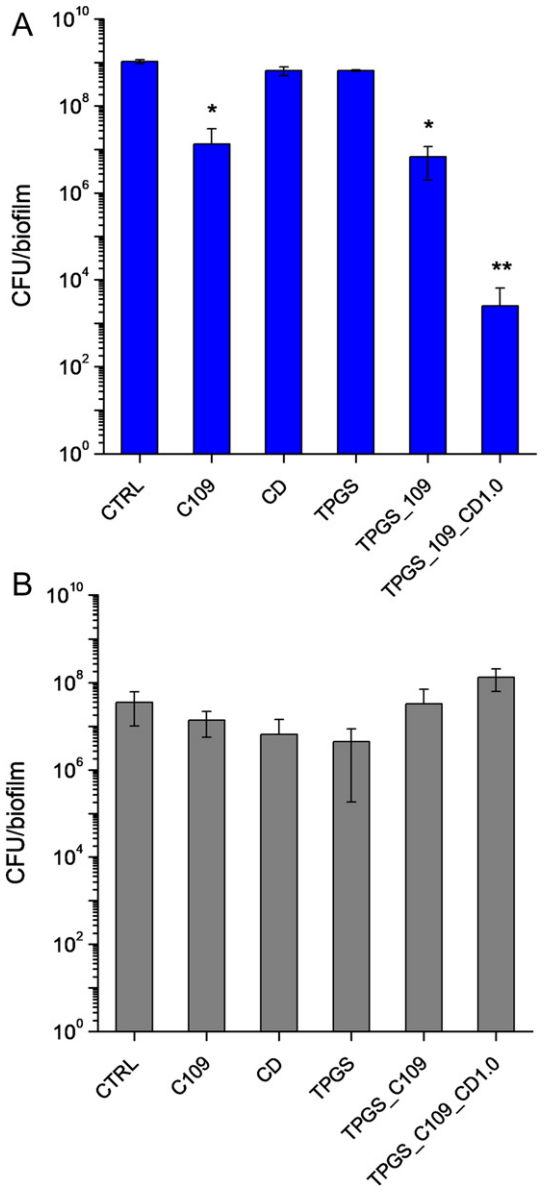

Figure 6. Inhibition (**A**) and eradication (**B**) ability of C109, TPGS_C109 or TPGS_C109_CD1.0 against *B. cenocepacia* J2315 biofilm. Data shown are the mean number of CFU recovered after no treatment (CTRL) or treatment with C109 (8 μg/mL) in DMSO (C109), TPGS_C109 or TPGS_C109_CD1.0. Error bars are SD calculated on triplicate experiments ($n = 3$). Data were analyzed by using a one-way ANOVA, with a Scheffe *post hoc* test (*$P < 0.05$ *versus* CTRL, **$P < 0.05$ *versus* C109).

in agreement with the sign of the nanosuspension concentration gradient. However, bold blue line also shows a lower intensity at low-q with respect to the orange one, possibly suggesting unbalanced contributions of the components, that is, uneven migration rates between the large nanocrystals and the small free components. Considering the 30% polydispersity in size of the nanocrystals in suspension, the entire set of data would be explained by assuming a counterintuitive higher diffusivity of crystals with larger sizes.

Finally, Figure 5, *B* shows a representative spectrum from a last scan of the capillary after 10 h delay: the low-q excess scattering reported by the orange bold spectrum just discussed, is no more seen. This observation provides further evidence of a deconstruction of the nanocrystal after long time in artificial *CF* mucus, consistently with SANS data.

Table 3
MIC determination (μg/ml) of C109 nanocrystal-embedded dry powders compared to C109.

Strain	TPGS_C109_CD0.5/ TPGS_C109_CD1.0	C109	Reference
B. cenocepacia J2315	8	8	Lab strain
B. cenocepacia K56-2	8	8	Lab strain
B. cenocepacia 451 (III-A)	4	4	10
B. cenocepacia 1232 (III-A)	8	8	10
B. cenocepacia 3167 (III-A)	16	32	10
B. cenocepacia FCF13 (III-A)	32	32	10
B. cenocepacia FCF14 (III-A)	8	8	10
B. cenocepacia FCF22 (III-B)	128	256	10
B. cenocepacia FCF23 (III-B)	16	16	10
B. cenocepacia FCF24 (III-B)	8	4	10
B. cenocepacia FCF27 (III-B)	8	4	10
B. cenocepacia FCF36 (III-D)	16	16	10
E. coli ATCC25922	4	8	11
A. baumannii ATCC 19606	8	16	11
S. aureus ATCC25923	2	4	11

Assessment of in vitro antimicrobial activity of C109 nanocrystals

The biological activity of the formulations was first assessed against planktonic *B. cenocepacia* cultures. The MICs of free C109, TPGS_C109_CD0.5 and TPGS_C109_CD1.0 were identical (Table 3). Moreover, time-kill curves of *B. cenocepacia* J2315 in the presence of C109 dissolved in DMSO or of formulated C109 are identical (Figure S4).

To further confirm the effectiveness of TPGS_C109_CD0.5 and TPGS_C109_CD1.0, MICs were determined also against a panel of *B. cenocepacia* clinical isolates representative of three genomovars (III-A, B, and D). The results were perfectly comparable to the one of the C109 compound dissolved in DMSO (Table 3). Also, the MICs of the formulations were determined for other Gram-negatives (*Escherichia coli*, *Acinetobacter baumannii*) and the Gram-positive *Staphylococcus aureus*, achieving the same results (Table 3).

It is noteworthy that *B. cenocepacia* can form biofilm, thus rendering the treatment of infections much more difficult. We compared the ability of C109, TPGS_C109 and freeze-dried powders containing the highest amount of CD (*i.e.*, TPGS_C109_CD1.0) to inhibit and eradicate biofilms at a concentration of 8 μg/ml (Figure 6). When it comes to inhibiting *B. cenocepacia* J2315 biofilms, C109 and TPGS_C109 resulted in a significant (*$P < 0.05$ *versus* CTR) approximately 100-fold (2 log) reduction of CFU/biofilm, while TPGS_C109_CD1.0 resulted in a 4-log reduction of CFU/biofilm as compared to C109 (**$P < 0.05$ *versus* C109) (Figure 6, *A*). Nevertheless, none of the compounds was able to eradicate the biofilm (Figure 6, *B*).

Cytotoxicity of C109 nanocrystals to CF bronchial epithelial cells

The cytotoxicity of the different C109 formulations against a wild type (16HBE) and a *CF* bronchial epithelial (CFBE41o$^-$)

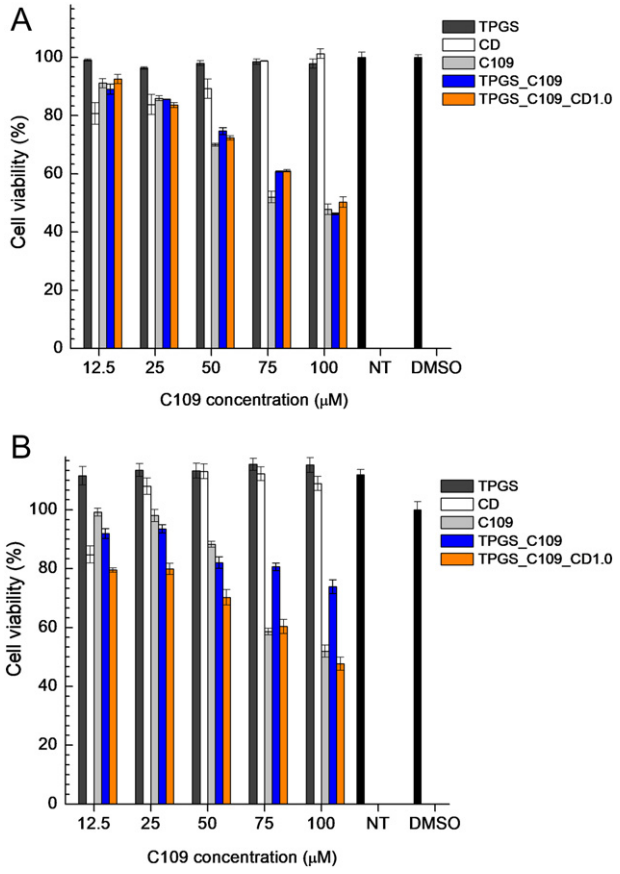

Figure 7. Cytotoxicity of C109 formulations to wild type 16HBE (**A**) and *CF* (CFBE41o$^-$) bronchial epithelial cells (**B**). Data are presented as mean value ± SD calculated on triplicate experiments (n = 3).

cell lines was assessed by the MTT assay. As previously shown, the toxic concentration at 50% (TC50) of C109 on these cell lines is about 75 μM.[11] C109 nanocrystals showed the same behavior as C109 compound in 16HBE cells (Figure 7, *A*), while the TC50 of TPGS_C109 was greater than 100 μM in CFBE41o$^-$ cells (Figure 7, *B*). The corresponding controls, TPGS and CD alone (Figure 7), as well as the combination of CD and TPGS (data not shown) did not cause significant toxicity. Of note, the TC50 of C109 and the corresponding TPGS_C109_CD1.0 was at least 3-fold higher than the microbiologically active concentration of the compound on the most sensitive bacterial strains, that is 13.5-27 μM (4–8 μg/mL) (Table 1). No differences were apparent between TPGS_C109_CD0.5 and TPGS_C109_CD1.0 (data not shown).

In vivo antimicrobial activity of C109 nanocrystals

The *in vivo* antimicrobial activity of the formulation alone or in combination with piperacillin, previously demonstrating *in vitro* additive interaction with C109 against K56-2,[11] was investigated.

Neither C109 or the formulation, or the antibiotic was toxic for *G. mellonella* at the concentrations used (data not shown). Larvae succumbed to the infection upon treatment with PS, DMSO, TPGS, C109 (data not shown) or TPGS_C109 or

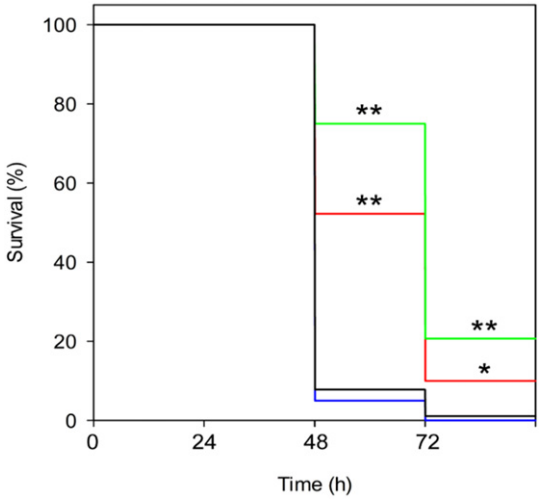

Figure 8. Kaplan–Meier survival-curve of infected *G. mellonella* receiving no treatment (black) or a treatment with piperacillin (red), the formulation TPGS_C109 (blue) or the combination piperacillin plus TPGS_C109_CD (green). ** $P < 0.01$; * $P < 0.05$. Survival curves were analyzed by using a log-rank (Mantel–Cox) test.

receiving no treatment (Figure 8) by 72 h post-infection (*p.i.*). On the contrary, when treated with piperacillin or the combination of piperacillin and TPGS_C109 survival was significantly increased after 48 and 72 h *p.i.* (Figure 8). Interestingly, the highest survival rate was achieved using the combination TPGS_C109 *plus* piperacillin (75% survival *versus* 52% of the piperacillin alone after 48 h, and 20% *versus* 10% after 72 h). The same result was not achieved when C109 compound was used in combination with piperacillin (data not shown).

These observations were confirmed by measuring the bacterial load (CFU/larva) at 48 and 72 h *p.i.*in the hemolymph of two larvae/group: only upon treatment with piperacillin alone or the combination piperacillin *plus* TPGS_C109 was the bacterial load significantly reduced (data not shown).

Discussion

B. cenocepacia is a resistant Gram-negative bacterium, carrying a worse prognosis and posing substantial therapeutic challenges to *CF* sufferers.[4] In this work, we propose an inhalable formulation for lung delivery of the poorly water-soluble FtsZ inhibitor C109, with promising activity against *B. cenocepacia*.[10,11]

Pulmonary delivery of poorly soluble actives may generate bioavailability and efficacy problems. Once deposited at lungs, undissolved drug particles are either cleared by the mucociliary escalator or phagocytized by alveolar macrophages.[35] Here, the reduction of particle size to the nanometer scale by nanoprecipitation increases surface C109 area exposed to lung lining fluids and drug saturation solubility at the solid surface. Nevertheless, the presence of TPGS was necessary to stabilize nanocrystal surface. TPGS is a generally recognized as safe water-soluble derivative of natural vitamin E,[36] the application of which encompasses also the stabilization of inhalable nanosuspensions.[37–39] Furthermore,

FALT measurements suggest a "complete mushroom" structure of PEG onto the nanocrystalline surface, likely contributing to nanosuspension stability *via* steric hindrance.[34,40]

Despite the stabilizer, nanocrystal growth in the nanosuspension is unavoidable due to the complex interplay of thermodynamics and molecular kinetics.[41,42] Hence, crystal growth or agglomeration can occur not only for the large interfaces and the high Gibbs free energy of the disperse system, but also due to Ostwald ripening effects.[41] Thus, drying of the liquid nanocrystal formulation is often required in conjunction with stabilizers to obtain long term stability.[42] To this purpose, the aqueous dispersion of C109 nanocrystals was further processed by freeze-drying to achieve a dry powder that could be reconstituted before use, that is "nanocrystal-embedded dry powders". However, the dehydration process may induce stresses to nanocrystals, which can be mitigated by the use of appropriate cryoprotectants.[43] In line with previous studies,[24,44] CD represented a valid tool to stabilize the PEGylated nanoparticulate system during freeze-drying, since it may also promote PEG chain extension on nanocrystal surface.[25] Notably, the colloidal properties of the system and the shell architecture were not affected by the lyophilization cycle. The shell thickness slightly increased in the presence of CD, likely due to its potential interactions with PEG chain.[45] Furthermore, WAXS analyses confirmed that the typical crystal distances of raw C109 are not altered in the particle production process.

The ability of the developed nanosuspension to assist drug deposition at lungs and to improve the solubility profile of C109 in lung lining fluids is the "*conditio sine qua non*" to advance the formulation to further *in vitro*/*in vivo* studies. Regarding lung deposition, nanosuspensions are commonly atomized into fine droplets *via* an appropriate nebulizer.[46] A critical quality attribute of the formulation for an efficient pulmonary deposition is the aerodynamic droplet size distribution, which needs to be assessed and maintained across the different inhalation devices.[47] We demonstrated that the developed nanosuspension may be efficiently delivered by both conventional jet nebulizers and portable vibrating mesh nebulizers, currently regarded as the first choice for development of new inhaled products.[48] Once deposited at lungs, a fast C109 dissolution in lung lining fluids can be likely expected based on *in vitro* release data, suggesting also the ability of nanocrystals to diffuse in the mucus gel layer. Results were confirmed by SAXS-assisted diffusion studies, which definitively highlighted the ability of C109 nanocrystals to diffuse in the mucus model.

The diffusion inside an adhesive gel, such as mucus, occurs in the presence of interaction forces between particle components and the building blocks of the hydrogel mesh, that is mucins and possibly DNA. The presence of a TPGS-derived brush PEG shell on the nanocrystal surface can reduce particle adhesion to mucin fibers found in the mucus mesh, thereby allowing the particles to quickly diffuse through the interstitial fluids between the fibers.[21] Nevertheless, some shape concerns may play an important role in promoting the diffusion of C109 nanocrystals, especially in view of the large particle size compared to the typical mucus mesh size (around 300 nm).[49,50] Recently, rod-like particle diffusivity in mucus was demonstrated to be higher than that of spherical particles with a diameter equal to the rod minor axis one.[51] The ability to diffuse is enforced by a preferred optimum aspect ratio of the elongated nanoparticles.[52] In fact, adhesive gel is thought to cause a jumping-diffusion path of the diffusant that enables rod-like particles of optimized aspect ratio to achieve higher diffusivity than spherical ones. A similar behavior can be hypothesized for the large elongated C109 nanocrystals, for which the aspect ratio may play the role of the selection parameter for diffusion inside the mucus mesh with a defined porosity.

Based on the encouraging physico-chemical and technological properties, C109 nanocrystals underwent further studies aimed at assessing their *in vitro* toxicological profile on human bronchial epithelial cells and antimicrobial activity against *B. cenocepacia*. Results highlighted how the broad-spectrum antimicrobial activity of C109 is maintained upon formulation and at microbiologically active concentrations the nanocrystals did not significantly affect the viability of both wild type and *CF* human bronchial epithelial cells. We previously showed that C109 was also effective at inhibiting biofilm formation of *B. cenocepacia*, but less capable of eradicating cells residing in established biofilms.[11] Results confirmed that C109 nanosuspensions significantly inhibited *B. cenocepacia* biofilm formation. Noteworthy, the inhibitory effect was much more pronounced in case of CD-containing nanocrystal-embedded dry powders. Based on previous evidences,[53] a potential entrapment of N-acyl homoserine lactones involved in bacterial quorum sensing inside CD cavity, likely contributing to C109 biofilm inhibitory activity, cannot be excluded.

A proof-of-concept of the *in vivo* potential of the C109 formulations in eradicating *B. cenocepacia* infections was finally given through the well-assessed *Galleria mellonella* model.[54] Results highlighted that neither the C109 compound nor formulation was toxic for *G. mellonella* and confirmed the biocompatibility of TPGS_C109 formulation in a complex physiological environment. While neither the raw compound nor the formulation was able to eradicate the *B. cenocepacia* infection, a significant improvement in survival was observed in larvae treated with both piperacillin and TPGS_C109. This clearly indicates a synergistic effect with a well-established drug and paves the way to the use of C109 nanocrystals as a local treatment option for combined therapy of *B. cenocepacia* lung infection.

Acknowledgments

G.R., F.U. and V.M. wish to thank the Italian Cystic Fibrosis Research Foundation (Project FFC #19/2015 adopted by *Gruppo di Sostegno FFC di Como Dongo, Delegazioni FFC di Olbia Tempio e di Reggio Calabria*) and the US Cystic Fibrosis Foundation (grant RICCAR17G0) for funding support. The work was supported also by a BlueSky research grant of the University of Pavia to S.B. and by the Italian Ministry of Education, University and Research (MIUR) (*Dipartimenti di Eccellenza, Program 2018-2022*) to Department of Biology and Biotechnology, "L. Spallanzani", University of Pavia (to G.R., S.B., L.R.C.). P.B. and V.R. were supported by research grant from BioMeTra Department of the University of Milano. P.B.

and V.R. benefitted from beam time by European Synchrotron Radiation Facility (ID02 beam line); beam time by Institut Laue-Langevin (ILL) doi:https://doi.org/10.5291/ILL-DATA.8-03-893; the use of the SasView application, originally developed under NSF award DMR-0520547. SasView contains code developed with funding from the European Union's Horizon 2020 research and innovation program under the SINE2020 project (Grant agreement no. 654000).

Appendix A. Supplementary data

Supplementary data to this article can be found online at https://doi.org/10.1016/j.nano.2019.102113.

References

1. Lyczak JB, Cannon CL, Pier GB. Lung infections associated with cystic fibrosis. *Clin Microbiol Rev* 2002;**15**:194-222.
2. Doring G, Flume P, Heijerman H, Elborn JS. Treatment of lung infection in patients with cystic fibrosis: current and future strategies. *J Cyst Fibros* 2012;**11**:461-79.
3. Ciofu O, Hansen CR, Hoiby N. Respiratory bacterial infections in cystic fibrosis. *Curr Opin Pulm Med* 2013;**19**:251-8.
4. Salsgiver EL, Fink AK, Knapp EA, LiPuma JJ, Olivier KN, Marshall BC, et al. Changing epidemiology of the respiratory bacteriology of patients with cystic fibrosis. *Chest* 2016;**149**:390-400.
5. Saiman L, Siegel J. Infection control recommendations for patients with cystic fibrosis: microbiology, important pathogens, and infection control practices to prevent patient-to-patient transmission. *Infect Control Hosp Epidemiol* 2003;**24**:S6-52.
6. Murray S, Charbeneau J, Marshall BC, LiPuma JJ. Impact of burkholderia infection on lung transplantation in cystic fibrosis. *Am J Respir Crit Care Med* 2008;**178**:363-71.
7. Dupont L. Lung transplantation in cystic fibrosis patients with difficult to treat lung infections. *Curr Opin Pulm Med* 2017;**23**:574-9.
8. Gibson RL, Burns JL, Ramsey BW. Pathophysiology and management of pulmonary infections in cystic fibrosis. *Am J Respir Crit Care Med* 2003;**168**:918-51.
9. Scoffone VC, Chiarelli LR, Trespidi G, Mentasti M, Riccardi G, Buroni S. Burkholderia cenocepacia infections in cystic fibrosis patients: drug resistance and therapeutic approaches. *Front Microbiol* 2017;**8**:1592.
10. Scoffone VC, Ryabova O, Makarov V, Iadarola P, Fumagalli M, Fondi M, et al. E ffl ux-mediated resistance to a benzothiadiazol derivative effective against Burkholderia cenocepacia. *Front Microbiol* 2015;**6**:815.
11. Hogan AM, Scoffone VC, Makarov V, Gislason AS, Tesfu H, Stietz MS, et al. Competitive fitness of essential gene knockdowns reveals a broad-spectrum antibacterial inhibitor of the cell division protein FtsZ. *Antimicrob Agents Chemother* 2018; AAC-18.
12. Lock RL, Harry EJ. Cell-division inhibitors: new insights for future antibiotics. *Nat Rev Drug Discov* 2008;**7**:324-38.
13. Smith S, Rowbotham NJ, Charbek E. Inhaled antibiotics for pulmonary exacerbations in cystic fibrosis. *Cochrane Database Syst Rev* 2018;**10**CD008319.
14. Rabinow BE. Nanosuspensions in drug delivery. *Nat Rev Drug Discov* 2004;**3**:785-96.
15. Shegokar R, Muller RH. Nanocrystals: industrially feasible multifunctional formulation technology for poorly soluble actives. *Int J Pharm* 2010;**399**:129-39.
16. Daniels T, Mills N, Whitaker P. Nebuliser systems for drug delivery in cystic fibrosis. *Cochrane Database Syst Rev* 2013CD007639.
17. d'Angelo I, Conte C, La Rotonda MI, Miro A, Quaglia F, Ungaro F. Improving the efficacy of inhaled drugs in cystic fibrosis: challenges and emerging drug delivery strategies. *Adv Drug Deliv Rev* 2014;**75**:92-111.
18. Murgia X, Loretz B, Hartwig O, Hittinger M, Lehr CM. The role of mucus on drug transport and its potential to affect therapeutic outcomes. *Adv Drug Deliv Rev* 2018;**124**:82-97.
19. Forier K, Messiaen AS, Raemdonck K, Deschout H, Rejman J, De BF, et al. Transport of nanoparticles in cystic fibrosis sputum and bacterial biofilms by single-particle tracking microscopy. *Nanomedicine (Lond)* 2013;**8**:935-49.
20. Hoang T, Zierden H, Date A, Ortiz J, Gumber S, Anders N, et al. Development of a mucoinert progesterone nanosuspension for safer and more effective prevention of preterm birth. *J Control Release* 2019;**295**:74-86.
21. Huckaby JT, Lai SK. PEGylation for enhancing nanoparticle diffusion in mucus. *Adv Drug Deliv Rev* 2018;**124**:125-39.
22. Daum N, Tscheka C, Neumeyer A, Schneider M. Novel approaches for drug delivery systems in nanomedicine: effects of particle design and shape. *Wiley Interdiscip Rev Nanomed Nanobiotechnol* 2012;**4**:52-65.
23. Mohwald M, Pinnapireddy SR, Wonnenberg B, Pourasghar M, Jurisic M, Jung A, et al. Aspherical, nanostructured microparticles for targeted gene delivery to alveolar macrophages. *Adv Healthc Mater* 2017;**6**.
24. Palma G, Conte C, Barbieri A, Bimonte S, Luciano A, Rea D, et al. Antitumor activity of PEGylated biodegradable nanoparticles for sustained release of docetaxel in triple-negative breast cancer. *Int J Pharm* 2014;**473**:55-63.
25. Conte C, Fotticchia I, Tirino P, Moret F, Pagano B, Gref R, et al. Cyclodextrin-assisted assembly of PEGylated polyester nanoparticles decorated with folate. *Colloids Surf B Biointerfaces* 2016;**141**:148-57.
26. Narayanan T, Sztucki M, Van VP, Leonardon J, Gorini J, Claustre L, et al. A multipurpose instrument for time-resolved ultra-small-angle and coherent X-ray scattering. *J Appl Cryst* 2018;**51**:1511-24.
27. Costabile G, d'Angelo I, Rampioni G, Bondi R, Pompili B, Ascenzioni F, et al. Toward repositioning niclosamide for antivirulence therapy of Pseudomonas aeruginosa lung infections: development of inhalable formulations through nanosuspension technology. *Mol Pharm* 2015;**12**:2604-17.
28. Marques MRC, Loebenberg R, Almukainzi M. Simulated biological fluids with possible application in dissolution testing. *Dissolut Technol* 2011;**18**:15-28.
29. Martin A, Takiff H, Vandamme P, Swings J, Palomino JC. Portaels F. a new rapid and simple colorimetric method to detect pyrazinamide resistance in mycobacterium tuberculosis using nicotinamide. *J Antimicrob Chemother* 2006;**58**:327-31.
30. Mosmann T. Rapid colorimetric assay for cellular growth and survival: application to proliferation and cytotoxicity assays. *J Immunol Methods* 1983;**65**:55-63.
31. Seed KD, Dennis JJ. Development of galleria mellonella as an alternative infection model for the Burkholderia cepacia complex. *Infect Immun* 2008;**76**:1267-75.
32. Puig-Rigall J, Grillo I. Dreiss CcA, Gonz+ílez-Gaitano G. Structural and spectroscopic characterization of TPGS micelles: disruptive role of cyclodextrins and kinetic pathways. *Langmuir* 2017;**33**:4737-47.
33. Hammouda B. A new Guinier-Porod model. *J Appl Cryst* 2010;**43**:716-9.
34. Sadzuka Y, Nakade A, Hirama R, Miyagishima A, Nozawa Y, Hirota S, et al. Effects of mixed polyethyleneglycol modification on fixed aqueous layer thickness and antitumor activity of doxorubicin containing liposome. *Int J Pharm* 2002;**238**:171-80.
35. Wauthoz N, Amighi K. Formulation strategies for pulmonary delivery of poorly soluble drugs. In: Nokhodchi A, Martin GP, editors. *Pulmonary drug delivery: advances and challenges. Hoboken (NJ)*. John Wiley & Sons, Inc.; 2015. p. 87-122.
36. Guo Y, Luo J, Tan S, Otieno BO, Zhang Z. The applications of vitamin E TPGS in drug delivery. *Eur J Pharm Sci* 2013;**49**:175-86.
37. Duret C, Wauthoz N, Sebti T, Vanderbist F, Amighi K. New inhalation-optimized itraconazole nanoparticle-based dry powders for the treatment of invasive pulmonary aspergillosis. *Int J Nanomedicine* 2012;**7**:5475-89.
38. Leung SS, Wong J, Guerra HV, Samnick K, Prud'homme RK, Chan HK. Porous mannitol carrier for pulmonary delivery of cyclosporine a nanoparticles. *AAPS J* 2017;**19**:578-86.

39. Rossi I, Sonvico F, McConville JT, Rossi F, Frohlich E, Zellnitz S, et al. Nebulized coenzyme Q10 nanosuspensions: a versatile approach for pulmonary antioxidant therapy. *Eur J Pharm Sci* 2018;**113**:159-70.
40. Pandey G, Mittapelly N, Banala VT, Mishra PR. Multifunctional glycoconjugate assisted nanocrystalline drug delivery for tumor targeting and permeabilization of lysosomal-mitochondrial membrane. *ACS Appl Mater Interfaces* 2018;**10**:16964-76.
41. Wang Y, Zheng Y, Zhang L, Wang Q, Zhang D. Stability of nanosuspensions in drug delivery. *J Control Release* 2013;**172**:1126-41.
42. Pawar VK, Singh Y, Meher JG, Gupta S, Chourasia MK. Engineered nanocrystal technology: in-vivo fate, targeting and applications in drug delivery. *J Control Release* 2014;**183**:51-66.
43. Malamatari M, Somavarapu S, Taylor KM, Buckton G. Solidification of nanosuspensions for the production of solid oral dosage forms and inhalable dry powders. *Expert Opin Drug Deliv* 2016;**13**:435-50.
44. Conte C, Costabile G, d'Angelo I, Pannico M, Musto P, Grassia G, et al. Skin transport of PEGylated poly(epsilon-caprolactone) nanoparticles assisted by (2-hydroxypropyl)-beta-cyclodextrin. *J Colloid Interface Sci* 2015;**454**:112-20.
45. Miro A, d'Angelo I, Nappi A, La MP, Biondi M, Mayol L, et al. Engineering poly(ethylene oxide) buccal films with cyclodextrin: a novel role for an old excipient? *Int J Pharm* 2013;**452**:283-91.
46. Jethara SI, Patel AD, Patel MR, Patel MS, Patel KR. Recent survey on nanosuspension: a patent overview. *Recent Pat Drug Deliv Formul* 2015;**9**:65-78.
47. Martin AR, Finlay WH. Nebulizers for drug delivery to the lungs. *Expert Opin Drug Deliv* 2015;**12**:889-900.
48. Pritchard JN, Hatley RH, Denyer J, Hollen DV. Mesh nebulizers have become the first choice for new nebulized pharmaceutical drug developments. *Ther Deliv* 2018;**9**:121-36.
49. Suk JS, Lai SK, Wang YY, Ensign LM, Zeitlin PL, Boyle MP, et al. The penetration of fresh undiluted sputum expectorated by cystic fibrosis patients by non-adhesive polymer nanoparticles. *Biomaterials* 2009;**30**:2591-7.
50. Duncan GA, Jung J, Hanes J, Suk JS. The mucus barrier to inhaled gene therapy. *Mol Ther* 2016;**24**:2043-53.
51. Yu M, Wang J, Yang Y, Zhu C, Su Q, Guo S, et al. Rotation-facilitated rapid transport of Nanorods in mucosal tissues. *Nano Lett* 2016;**16**:7176-82.
52. Wang J, Yang Y, Yu M, Hu G, Gan Y, Gao H, et al. Diffusion of rod-like nanoparticles in non-adhesive and adhesive porous polymeric gels. *J Mech Phys Solids* 2018;**112**:431-57.
53. Brackman G, Garcia-Fernandez MJ, Lenoir J, De ML, Remon JP, De BT, et al. Dressings loaded with cyclodextrin-hamamelitannin complexes increase Staphylococcus aureus susceptibility toward antibiotics both in single as well as in mixed biofilm communities. *Macromol Biosci* 2016;**16**:859-69.
54. Thomas RJ, Hamblin KA, Armstrong SJ, Muller CM, Bokori-Brown M, Goldman S, et al. Galleria mellonella as a model system to test the pharmacokinetics and efficacy of antibiotics against Burkholderia pseudomallei. *Int J Antimicrob Agents* 2013;**41**:330-6.